



# Functionalization of ZrO<sub>2</sub> nanofibers with Pt nanostructures: The effect of surface roughness on nucleation mechanism and morphology control

Eric Formo<sup>a</sup>, Pedro H.C. Camargo<sup>a</sup>, Byungkwon Lim<sup>a</sup>, Majiong Jiang<sup>b</sup>, Younan Xia<sup>a,\*</sup>

<sup>a</sup> Department of Biomedical Engineering, Washington University, St. Louis, MO 63130, United States

<sup>b</sup> Department of Chemistry, Washington University, St. Louis, MO 63130, United States

## ARTICLE INFO

### Article history:

Received 13 May 2009

In final form 29 May 2009

Available online 6 June 2009

## ABSTRACT

ZrO<sub>2</sub> nanofibers with different surface roughness were employed as supports for the deposition of Pt nanostructures. When the nanofibers had a smooth surface, both homogeneous and heterogeneous nucleation took place, producing Pt nanoparticles deposited on the nanofibers and free-standing Pt nano-stars in the solution. By reducing the concentration of Pt precursor, Pt nanowires were formed on the nanofibers. For nanofibers with a rough surface, Pt nanoparticles were formed on the nanofibers through heterogeneous nucleation. These results demonstrate that the surface roughness had a significant impact on the nucleation mechanism and the morphology of the resultant Pt nanostructures.

© 2009 Elsevier B.V. All rights reserved.

## 1. Introduction

Platinum (Pt) is an invaluable catalyst in a wealth of industrial applications, including the CO/NO<sub>x</sub> oxidation in catalytic converters, production of nitric acid, petroleum cracking, and hydrogenation reactions [1]. Moreover, Pt is by far the most effective electrocatalyst for both the oxygen reduction reaction (ORR) and oxidation of the fuel (e.g., hydrogen, methanol, ethanol, and formic acid) in fuel cell technologies [2]. These applications demand the utilization of Pt in a finely divided state, in which the activity and/or selectivity of Pt-based catalysts can be greatly improved by controlling the size, shape, and morphology [3]. Therefore, tremendous efforts have been directed towards the synthesis of Pt nanostructures with well-controlled shapes (or facets), including nanocubes, octahedrons, tetrahedrons, nanowires, multipods, and nanostars [3].

For practical applications in heterogeneous catalysis, Pt nanostructures are usually deposited on a solid support in order to achieve their homogeneous dispersion and thus maximum possible surface site availability [4]. To this end, ceramic supports provide a robust platform for the incorporation of noble-metal nanoparticles [5]. The utilization of oxide supports such as TiO<sub>2</sub>, SnO<sub>2</sub>, CeO<sub>2</sub> and ZrO<sub>2</sub>, for example, have shown great promise to prevent aggregation and improve CO tolerance of Pt-based catalysts, thus enhancing their long term stabilities [6–11].

Electrospun nanofibers have proven to be effective catalytic supports owing to their high porosity and large surface area. The high porosity of a nonwoven mat of nanofibers usually enables direct growth of catalytic nanostructures via heterogeneous nucle-

ation. The successful use of electrospun nanofibers as supports for catalytic nanoparticles has been demonstrated for a number of reactions [12–15]. Previously, we have developed a method for depositing Pt nanostructures on the electrospun nanofibers made of TiO<sub>2</sub> and ZrO<sub>2</sub> through a simple polyol reduction approach, in which the nanofibers were added to a polyol reduction bath containing PVP and [PtCl<sub>6</sub>]<sup>2-</sup> [16,17]. In this method, the reduction of [PtCl<sub>6</sub>]<sup>2-</sup> generates Pt atoms that nucleate and grow onto the surface of the nanofibers. In our previous studies, the nanofibers were calcined at 550 °C for at least 6 h in order to obtain the surface roughness suitable for heterogeneous nucleation of the Pt atoms [16,17]. Here, we would like to investigate how shorter calcination times would affect the deposition of Pt nanostructures over the ZrO<sub>2</sub> nanofibers. The utilization of shorter calcination times, for example, would be very attractive from an economic point of view in the large-scale production of the supported catalyst. On the other hand, a shorter calcination time is expected to generate nanofibers with a smoother surface, which may have a strong impact on the nucleation (homogeneous vs. heterogeneous) of Pt atoms. The occurrence of homogeneous nucleation during the deposition step, for example, could lead to lower density of nanoparticle coating on the nanofibers and aggregation of the nanoparticles in the solution phase, causing detrimental effects over the catalytic performance [18].

In this work, we report on the utilization of a nonoven mat composed of ZrO<sub>2</sub> nanofibers having a smooth surface as a support for the deposition of Pt nanostructures via a polyol reduction approach. Here, the calcination temperature and time were reduced to 500 °C and 3 h, respectively, and the conditions for Pt deposition were similar to those reported in our previous studies (conducted with nanofibers calcined at 550 °C for 6 h). Interestingly, we found that the surface roughness of electrospun ZrO<sub>2</sub> nanofibers had a

\* Corresponding author.

E-mail address: [xia@biomed.wustl.edu](mailto:xia@biomed.wustl.edu) (Y. Xia).

significant impact not only on the nucleation mechanism, but also on the morphology of the resultant Pt nanostructures.

## 2. Experimental

### 2.1. Fabrication of $ZrO_2$ nanofibers by electrospinning

The fabrication of  $ZrO_2$  nanofibers was achieved by electrospinning a solution containing 1.5 g zirconium acetylacetonate (Aldrich), 1 mL acetic acid (EMD), 0.15 g PVP ( $M_w \approx 1.3 \times 10^6$ , Aldrich), and 2.5 mL ethanol (Pharmco). The solution was passed through a syringe with a 21 gauge stainless steel needle at the tip. The needle was electrified using a high-voltage DC power supply (ES30P-5 W, Gamma High Voltage Research Inc., Ormond Beach, FL) and a voltage of 20 kV was applied. The solution was injected continuously using a syringe pump (KDS-200, Stoelting, Wood Dale, IL) at a rate of 0.4 mL/h. The nanofibers were collected on a grounded aluminum foil and left overnight in air to fully hydrolyze. The as-prepared composite nanofibers containing amorphous  $ZrO_2$  and PVP were then calcined in air at 500 °C for 3 h to generate the polycrystalline ceramic fibers. For comparison, another batch of  $ZrO_2$  nanofibers was prepared following the same procedure, with the exception that the calcination step was conducted at 550 °C for 6 h.

### 2.2. Functionalization of the $ZrO_2$ nanofibers with Pt nanostructures

In a typical procedure, 4 mL of ethylene glycol (EG, J.T. Baker) containing 10 mg of  $ZrO_2$  nanofibers was injected into a 3-neck flask fitted with a reflux condenser and a Teflon-coated stir bar, followed by heating in air at 110 °C for 1 h. 400 mM PVP ( $M_w \approx 5.5 \times 10^4$ , Aldrich) and 80 mM  $H_2PtCl_6$  (Aldrich) were dissolved separately in 1 mL aliquots of EG at room temperature. These two solutions were then added simultaneously into the flask over a period of 1.5 min. The reaction mixture was further heated at 110 °C for 15 h. The final samples were washed thoroughly with

ethanol and water to remove EG and excess PVP. In order to investigate the effect of the concentration of Pt precursor on the nucleation and morphology of the deposited Pt nanostructures, the same procedure was used, with the exception that the initial concentrations of PVP and  $H_2PtCl_6$  were decreased to 200 mM and 40 mM, respectively.

### 2.3. Characterization

The SEM samples were prepared by placing a drop of the material onto a silicon substrate and allowing it to dry under ambient conditions. Images were taken using a field-emission SEM (FEI NovaNano 230, Hillsboro, OR) operated at an accelerating voltage of 5 kV for the  $ZrO_2$  nanofibers and 15 kV for the  $ZrO_2$  nanofibers after Pt functionalization. X-ray diffraction was conducted with a Geigerflex D-MAX/A Diffractometer (Rigaku, Berlin, Germany) using Cu-K radiation at 35 kV and 35 mA. The TEM samples were prepared by drop-casting a dispersion of the fibers onto carbon-coated copper grids (Formvar/Carbon, 200 mesh, Ted Pella). TEM images were acquired using a Tecnai G2 Spirit Twin (FEI, Hillsboro, OR) operated at 120 kV. High-resolution HRTEM was performed using a JEM-2100F (JEOL, Tokyo, Japan) operated at 200 kV.

## 3. Results and discussion

The  $ZrO_2$  nanofibers were prepared using a previously developed protocol, which involves electrospinning a polymer solution containing a sol-gel precursor (zirconium acetylacetonate) onto a flat grounded electrode in the form of a nonwoven mat [17,19]. Fig. 1A shows SEM image of the nonwoven mat of  $ZrO_2$  nanofibers that were generated after calcination at 500 °C for 3 h. As depicted in Fig. 1A, the nanofibers were uniform and their diameter was ~150 nm. The XRD pattern confirmed that the  $ZrO_2$  nanofibers were crystallized in the tetragonal phase (Fig. 1B). The TEM image (Fig. 1C) confirms that the nanofiber had a smooth and regular surface that was composed of nanocrystalline grains <5 nm in size. It

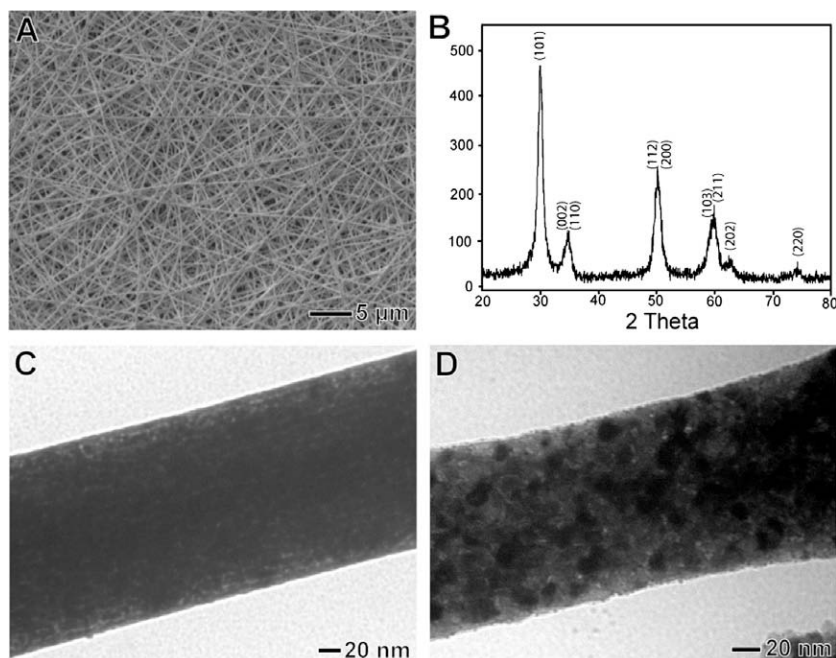


**Fig. 1.** (A) SEM image and (B) XRD pattern for the nonwoven mat of  $ZrO_2$  nanofibers prepared by calcination in air at 500 °C for 3 h. (C) TEM image of an individual  $ZrO_2$  nanofiber from the product displayed in (A). In this case, the surface of the nanofibers was smooth and made of nanocrystalline grains <5 nm in size. (D) TEM image of an individual  $ZrO_2$  nanofiber that was obtained after calcination at 550 °C for 6 h. In this case, the  $ZrO_2$  nanofiber displayed a rough and irregular surface comprised of bigger crystalline grains.

is worth pointing out that the calcination at 500 °C for 3 h resulted in some substantial differences over the ZrO<sub>2</sub> nanofiber surface morphology as compared to calcination at 550 °C for 6 h. As shown in Fig. 1D and previously reported by our group, the ZrO<sub>2</sub> nanofibers that were calcined at 550 °C for 6 h presented a significantly rough and irregular surface together with increased crystallite sizes [17].

After the ZrO<sub>2</sub> nanofibers had been synthesized, they could undergo a simple and versatile post-treatment approach to allow the deposition of Pt nanostructures onto their surface. In this case, the deposition of Pt onto the nanofibers was accomplished by immersing the nanofibers into a polyol reduction bath containing [PtCl<sub>6</sub>]<sup>2-</sup> and PVP for 15 h [3,20]. In our initial studies, we employed similar conditions as those previously reported for the ZrO<sub>2</sub> nanofibers that had been calcined at 550 °C for 6 h [17]. Fig. 2 A and B, displays TEM images of the resultant ZrO<sub>2</sub> nanofibers after their post-treatment in a polyol reduction bath. It can be observed that Pt nanoparticles 5 nm in diameter were deposited on the surface of the nanofiber as a packed array with a sub-monolayer coverage. In addition to their incomplete coverage, regions containing small aggregates of Pt nanoparticles were observed on the surface of the nanofiber (Fig. 2B). Interestingly, Pt nanostars (branched Pt

nanostructures) were co-produced in solution during the deposition step, as shown in Fig. 2C. Here, each Pt nanostar contained 2–6 branches, rounded edges and an overall size of 10 nm. HRTEM images of the Pt nanostars (Fig. 2D) revealed that they were single-crystalline, suggesting that they were formed via an overgrowth mechanism rather than through random aggregation of pre-formed small particles. It is important to note that the Pt nanostars could be easily isolated from the other materials by simply passing the reaction solution through a 200 nm membrane filter, which was able to selectively collect the relatively large Pt-decorated nanofibers.

These results suggest that both homogeneous and heterogeneous nucleation took place when ZrO<sub>2</sub> nanofibers having a smooth surface were employed as a support for the deposition of Pt nanostructures via a polyol approach. Specifically, the Pt atoms nucleated both in solution and on the nanofiber surface. After the nucleation step, as more Pt atoms were produced by the reduction of [PtCl<sub>6</sub>]<sup>2-</sup>, the seeds that had nucleated onto the surface of the nanofiber (via heterogeneous nucleation) grew until they became 5 nm in diameter. Meanwhile, an overgrowth mechanism was observed for the seeds that self-nucleated in solution, leading to the formation of the Pt nanostars. In this case, the evolution to a

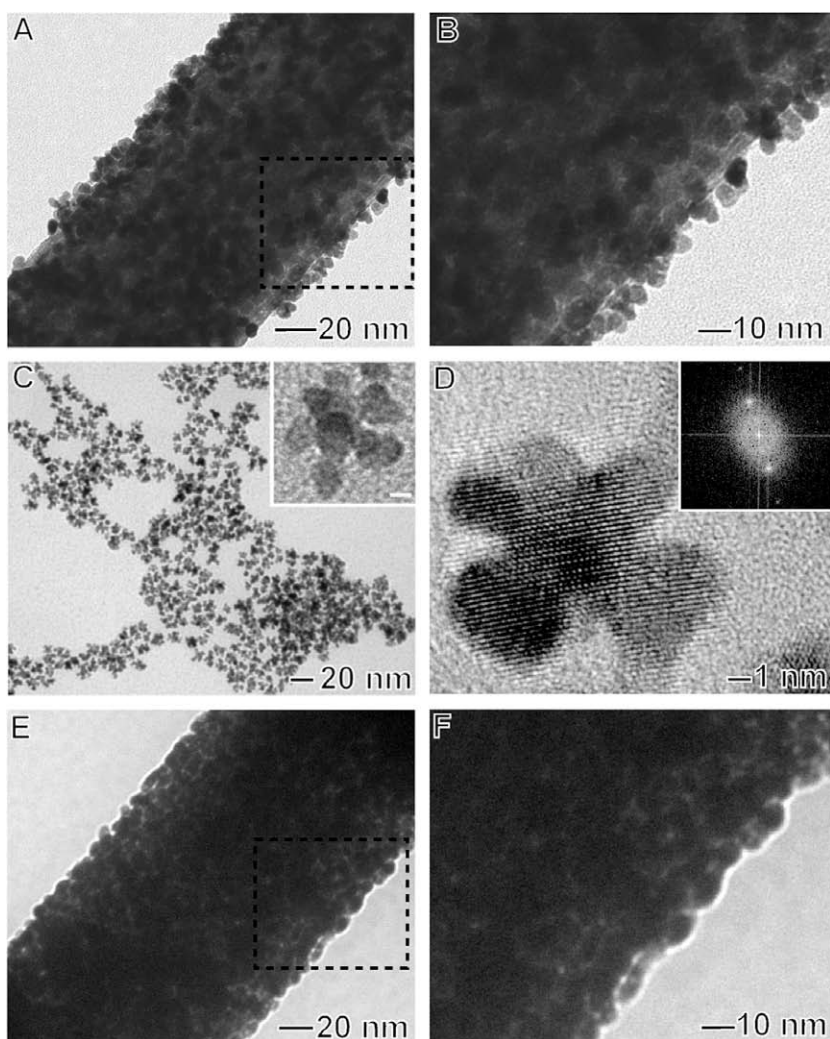


**Fig. 2.** (A and B) TEM images of an individual ZrO<sub>2</sub> nanofiber (calcined at 500 °C for 3 h) that was coated with Pt nanoparticles by immersing the nanofibers in a polyol reduction bath for 15 h. (C) TEM image of the Pt nanostars 10 nm in size that were co-produced in solution during the Pt deposition step. The scale bar in the inset corresponds to 2 nm. (D) HRTEM image of a Pt nanostar, revealing that they were single-crystalline. (E and F) TEM images of an individual ZrO<sub>2</sub> nanofiber that was calcined at 550 °C for 6 h and coated with Pt nanoparticles using a similar method as described in (A).

branched morphology seems to result from the overgrowth of initially formed cuboctahedral Pt seeds at their corner sites. The overgrowth mechanism for Pt nanostructures has been observed at low concentration of seeds and high concentration of Pt atoms [20–25]. In our system, it is plausible that the concentration of seeds formed in solution via homogeneous nucleation was relatively low enough as compared to the concentration of the generated Pt atoms during the reduction of  $[\text{PtCl}_6]^{2-}$ . As some Pt seeds had been formed in solution, further generation of Pt atoms could be accelerated via an autocatalytic process, contributing to sustain their high concentration in solution and enable the overgrowth mechanism [21–26].

It is important to note that only heterogeneous nucleation was favored when nanofibers with a rough surface (calcined for at 550 °C for 6 h) were used under similar experimental conditions. In this case, the TEM images of the Pt-decorated nanofibers (Fig. 2E and F) indicate that their surface was completely covered by a sheath of densely packed Pt nanoparticles and no material was co-produced in the solution. The higher coverage of Pt nanoparticles on the  $\text{ZrO}_2$  nanofibers supports this observation (Fig. 2F). Fig. 3 shows a schematic summarizing the effect of the nanofiber's surface roughness on the deposition of Pt nanostructures. It has been reported that highly irregular and rough surface can serve as primary nucleation sites for the growth of noble-metal nanostructures because of the higher surface energies associated with irregularities such as indentions, step edges, or protrusions which significantly lower the barrier for heterogeneous nucleation [27,28]. Therefore, for  $\text{ZrO}_2$  nanofibers with a rough surface (Fig. 3A), the increased number of nucleation sites for the deposition of Pt atoms associated with the increased surface area of the nanofiber enables heterogeneous nucleation to become more favorable while homogeneous nucleation was suppressed. Conversely, when the nanofiber surface was relatively smooth and regular (Fig. 3B), its corresponding lower surface area provided a significantly lower number of nucleation sites for the growth of Pt nanostructures. Under the experimental conditions we used, it is possible that the energy barrier for heterogeneous nucleation could not be lowered enough so that homogeneous nucleation would be suppressed, enabling both homogeneous and heterogeneous nucleation to occur.

In order to explore the effect of the concentration of Pt precursor on the formation of Pt nanostructures, we decided to decrease the concentration of  $[\text{PtCl}_6]^{2-}$  employed in the polyol reduction

bath. Fig. 4 displays the product obtained after the  $\text{ZrO}_2$  nanofibers were immersed in a polyol reduction bath for 15 h, in which the concentration of  $[\text{PtCl}_6]^{2-}$  and PVP were decreased by two times as compared to the product depicted in Fig. 2. Fig. 4A and B, shows SEM images of the product, indicating that it was comprised of agglomerate structures composed of Pt nanowires supported on the  $\text{ZrO}_2$  nanofibers. From these images, it is clear that the as-prepared Pt nanowires were uniform in size distribution. Moreover, regions containing only the bare  $\text{ZrO}_2$  nanofiber could be observed in the image. Fig. 4C shows a TEM image of the Pt nanowires located at the surface of the Pt agglomerates, indicating that the nanowires were 5 nm in diameter, with lengths up to 120 nm. The HRTEM image (Fig. 4D) confirmed that the nanowire grew along the  $\{1\ 1\ 1\}$  direction. We have previously observed similar hierarchically agglomerate structures containing Pt nanowires that were formed upon the addition of  $\text{Fe}^{2+}$  or  $\text{Fe}^{3+}$  species into polyol synthesis of Pt nanostructures [20,29,30]. In our previous studies, the  $\text{Fe}^{2+}/\text{Fe}^{3+}$  pair acted as an oxidative etchant that was able to oxidize the Pt atoms and nuclei back to  $\text{Pt}^{\text{II}}$ . This reduction in the number of Pt atoms in the solution forced the reduction kinetics to an extremely slow rate, inducing the Pt atoms to nucleate and grow into uniform nanowires. Interestingly, here we observed the formation of hierarchically structures containing Pt nanowires in the presence of  $\text{ZrO}_2$  nanofibers without the introduction of any  $\text{Fe}^{2+}/\text{Fe}^{3+}$  species. It is possible that, by decreasing the concentration of  $[\text{PtCl}_6]^{2-}$  (thus decreasing the number of Pt seeds), the subsequent reduction reaction to produce Pt atoms could be slowed down below a critical level that was sufficient to induce anisotropic growth. In this case, the decrease in the concentration of Pt seeds (by decreasing the concentration of Pt precursor) would have a similar effect over the reduction kinetics as the addition of  $\text{Fe}^{2+}/\text{Fe}^{3+}$  species into the polyol bath. Also, as  $[\text{PtCl}_6]^{2-}$  releases  $\text{Cl}^-$  into the reaction solution during the formation of Pt atoms, it is possible that the  $\text{O}_2/\text{Cl}^-$  pair could have acted as an oxidative etchant, contributing to the slow down of reduction kinetics that led to anisotropic growth [26,31–33]. The mechanism for the production of Pt nanowires may involve overgrowth on one of the eight  $\{1\ 1\ 1\}$  facets of a cuboctahedral seed via an autocatalytic process. Another mechanism would involve the formation of long chain  $\text{Pt}^{\text{II}}$  or  $\text{Pt}^{\text{IV}}$  complexes such as  $[\text{PtCl}_4]^{2-}$  or its water-substituted form  $[\text{PtCl}_4(\text{H}_2\text{O})_2]^{2-}$  prior to their reduction to Pt atoms. Upon reduction, these long chain complexes could evolve into the nanowires.

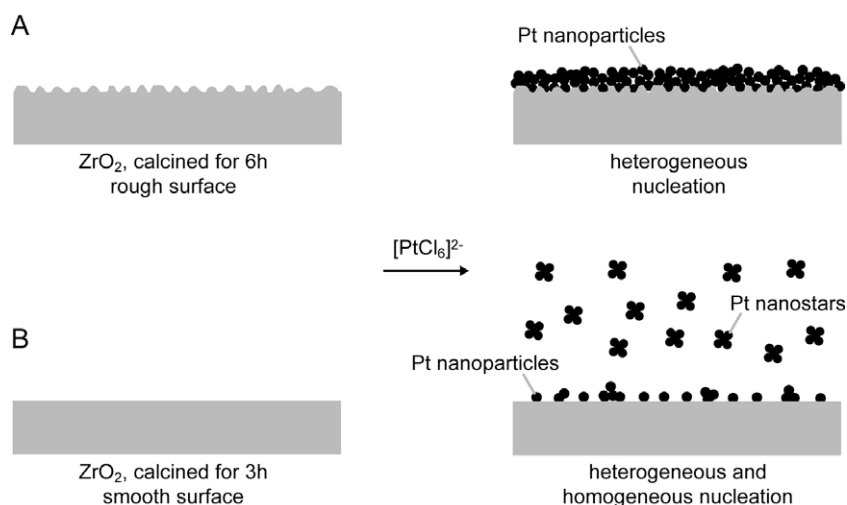


**Fig. 3.** A schematic summarizing the effect of surface roughness on the deposition of Pt nanostructures. (A) When the nanofibers had a rough and irregular surface, Pt nanoparticles were deposited via heterogeneous nucleation over the nanofiber's surface as a densely packed array or a complete sheath. (B) Conversely, when the nanofibers had a relatively smooth surface, both homogeneous and heterogeneous nucleation was observed. While the heterogeneous nucleation led to the decoration of the nanofibers with Pt nanoparticles 5 nm in size as a sub-monolayer, homogeneous nucleation resulted in the formation of free-standing Pt nanostars.

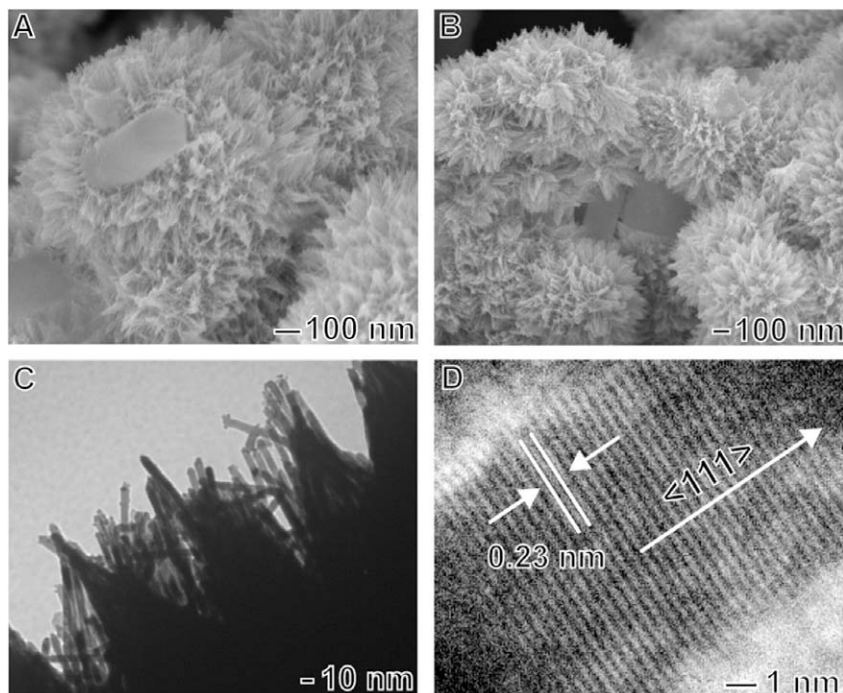


**Fig. 4.** (A and B) SEM images of the product obtained by decreasing the concentration of  $[\text{PtCl}_6]^{2-}$  by two times. Here, hierarchical agglomerates composed of Pt nanowires supported on the  $\text{ZrO}_2$  nanofibers were produced. (C) TEM image taken from the surface of an agglomerate, depicting that the Pt nanowires were uniform and had a diameter of 5 nm and lengths up to 120 nm. (D) HRTEM of an individual Pt nanowire, indicating that growth took place along the  $\{111\}$  direction.

It is important to note that this could also explain why the growth direction for the nanowires was different from those observed for other *fcc* noble-metals (that typically grow along the  $\{100\}$  direction) [3,34–37]. The formation of agglomerate structures containing Pt nanowires supported on the  $\text{ZrO}_2$  nanofibers may also involve both homogeneous and heterogeneous nucleation. In this case, the produced Pt atoms nucleated both onto the nanofiber surface and in the solution. As the overall number of seeds produced during the nucleation step was decreased (due to a lower concentration of Pt precursor), anisotropic growth was induced. The Pt nanowires then aggregated both in solution and onto the nanofiber's surface to produce micrometer-sized agglomerate structures containing Pt nanowires together with the nanofibers. Interestingly, Pt nanowires were not obtained when nanofibers with a rough surface (calcined for at  $550^\circ\text{C}$  for 6 h) were employed under similar experimental conditions. In this system, only heterogeneous nucleation took place and the product was composed of  $\text{ZrO}_2$  nanofibers decorated with Pt nanoparticles.

#### 4. Summary

We have examined the utilization of  $\text{ZrO}_2$  nanofibers as a support for the deposition of Pt nanostructures through a polyol reduction approach. When the nanofibers had a rough and irregular surface, heterogeneous nucleation took place and the nanofibers could be readily functionalized with a complete sheath composed of densely packed array of Pt nanoparticles. Conversely, when the nanofibers had a smooth surface, both homogeneous and heterogeneous nucleation was observed under similar experimental conditions. While heterogeneous nucleation led to the decoration of the nanofibers with Pt nanoparticles 5 nm in size with a sub-monolayer coverage, homogeneous nucleation led to the formation of Pt nanostars 10 nm in size via an overgrowth mechanism. Moreover, when the concentration of Pt precursor was reduced by two times, agglomerate structures composed of Pt

nanowires supported on the  $\text{ZrO}_2$  nanofibers were formed. In this case, the reduction kinetics could be slowed down below a critical level that was sufficient to induce anisotropic growth by simply decreasing the number of Pt seeds produced during the nucleation step. The results presented herein suggest that the surface roughness of the support  $\text{ZrO}_2$  nanofibers had a profound impact not only on the Pt nucleation mechanism, but also the morphology of the resultant Pt nanostructures.

#### Acknowledgements

This work was supported by a research grant from the NSF (DMR-0804088) and startup funds from Washington University in St. Louis. P.H.C.C. was partially supported by the Fulbright Program and the Brazilian Ministry of Education (CAPES).

#### References

- [1] G. Ertl, Handbook of Heterogeneous Catalysis, Wiley-VCH, Weinheim, 2008.
- [2] H.A. Gasteiger, S.S. Kocha, B. Sompalli, F.T. Wagner, Appl. Catal. B: Environ. 56 (2005) 9.
- [3] J. Chen, B. Lim, E. Lee, Y. Xia, Nano Today 4 (2009) 81.
- [4] X.W. Yu, S.Y. Ye, J. Power Sources 172 (2007) 145.
- [5] X. He, D. Antonelli, Angew. Chem. Int. Ed. 41 (2002) 214.
- [6] M. Gustavson, H. Ekstrom, P. Hanarp, L. Eurenium, G. Lindbergh, E. Olsson, B. Kasemo, J. Power Sources 163 (2007) 671.
- [7] M. Heipel, I. Dela, T. Heipel, J. Luo, C. Zhong, Electrochim. Acta 52 (2007) 5529.
- [8] L. Yang, W. Yang, Q. Cai, J. Phys. Chem. C 111 (2007) 16613.
- [9] L. Jiang et al., J. Phys. Chem. B 109 (2005) 8774.
- [10] J.R. Croy, S. Mostafa, J. Liu, Y. Sohn, H. Heinrich, B.R. Cuenya, Catal. Lett. 119 (2007) 209.
- [11] M.V.M. Souza, N.F.P. Ribeiro, M. Schmal, Int. J. Hydrogen Energ. 32 (2007) 425.
- [12] M. Graeser, E. Pippel, A. Greiner, J. Wendroff, Macromolecules 40 (2007) 6032.
- [13] S. Zhan, D. Chen, X. Jiao, Y. Song, Chem. Commun. 20 (2007) 2043.
- [14] A. Patel, S. Li, C. Wang, W. Zhang, Y. Wei, Chem. Mater. 19 (2007) 1231.
- [15] M.M. Demir et al., Macromolecules 37 (2004) 1787.
- [16] E. Formo, E. Lee, D. Campbell, Y. Xia, Nano Lett. 8 (2008) 668.
- [17] E. Formo, M.S. Yavuz, E.P. Lee, L. Lane, Y. Xia, J. Mater. Chem. 19 (2009) 3878.
- [18] B.C. Gates, Chem. Rev. 95 (1995) 511.
- [19] D. Li, Y. Xia, Nano Lett. 3 (2003) 555.
- [20] J. Chen, T. Herricks, Y. Xia, Angew. Chem. Int. Ed. 44 (2005) 2589.

- [21] J. Ren, R.D. Tilley, *J. Am. Chem. Soc.* 129 (2007) 3287.
- [22] M.A. Mahmoud, C.E. Tabor, M.A. El-Sayed, Y. Ding, Z.L. Wang, *J. Am. Chem. Soc.* 130 (2008) 4590.
- [23] B. Lim, X. Lu, M. Jiang, P.H.C. Camargo, E.C. Cho, E.P. Lee, Y. Xia, *Nano Lett.* 8 (2008) 4043.
- [24] J. Ren, R.D. Tilley, *Small* 3 (2007) 1508.
- [25] T. Herricks, J. Chen, Y. Xia, *Nano Lett.* 4 (2004) 2367.
- [26] Y. Xia, Y. Xiong, B. Lim, S. Skrabalak, *Angew. Chem. Int. Ed.* 48 (2009) 60.
- [27] A. Gouldstone, K.J. Van Vliet, S. Suresh, *Nature* 411 (2001) 656.
- [28] H. Brune, *Surf. Sci. Rep.* 31 (1998) 121.
- [29] E.P. Lee, Z. Peng, D.M. Cate, H. Yang, C.T. Campbell, Y. Xia, *J. Am. Chem. Soc.* 129 (2007) 10634.
- [30] J. Chen, T. Herricks, M. Geissier, Y. Xia, *J. Am. Chem. Soc.* 126 (2004) 10854.
- [31] B. Wiley, T. Herricks, Y. Sun, Y. Xia, *Nano Lett.* 4 (2004) 1733.
- [32] Y. Xiong, J. Chen, B. Wiley, Y. Xia, S. Aloni, Y. Yin, *J. Am. Chem. Soc.* 127 (2005) 7332.
- [33] B. Wiley, Y. Sun, Y. Xia, *Langmuir* 21 (2005) 8077.
- [34] L. Colombi Ciacchi, W. Pompe, A. De Vita, *J. Am. Chem. Soc.* 123 (2001) 7371.
- [35] M. Mertig, L.C. Ciacchi, R. Seidel, W. Pompe, A. De Vita, *Nano Lett.* 2 (2002) 841.
- [36] L.C. Ciacchi, M. Mertig, W. Pompe, S. Meriani, A. De Vita, *Platinum Met. Rev.* 47 (2003) 98.
- [37] L.C. Ciacchi, W. Pompe, A. De Vita, *J. Phys. Chem. B* 107 (2003) 1755.